Uncertainty Quantification of Thermal Damage in Hyperthermia as a Cancer Therapy

Gustavo Coelho Martins[1[0009−0004−1725−4135]], Gustavo Resende Fatigate[2[0000−0002−2600−2974]] Marcelo Lobosco[1,2[0000−0002−7205−9509]], and Ruy Freitas Reis[1,2⋆[0000−0001−5215−3744]]

[1] Departamento de Ciência da Computação, Universidade Federal de Juiz de Fora, Brazil
[2] Pós-Graduação em Modelagem Computacional, Universidade Federal de Juiz de Fora, Brazil
ruy.reis@ufjf.br

Abstract. Hyperthermia is a minimally invasive auxiliary cancer treatment that induces tumor damage and cell death by elevating tissue temperatures. The Arrhenius model is commonly used to evaluate thermal damage in biological tissues. However, variability in key Arrhenius parameters, such as frequency factor (A) and activation energy (E_a), can compromise the therapy planning. This study quantifies how these uncertain inputs might affect the simulation results. So, we consider a three-dimensional breast tissue model governed by Pennes' bioheat equation, considering different values of A and E_a found in the literature. Moreover, this study performs the uncertainty quantification analysis via Monte Carlo simulations using a GPU-accelerated implementation. Our results show that uncertainty in A contributes minimally to the damage integral Ω_A. In contrast, variability in E_a broadens the 95% confidence interval for the critical threshold ($\Omega_A \geq 4$), extending the required treatment time from approximately 15 to 35 minutes. These remarks highlight the necessity of precise E_a estimation to ensure reliable hyperthermia protocols.

Keywords: Hyperthermia · Cancer · Bioheat · Uncertainty Quantification · High Performance Computing

1 Introduction

Cancer refers to a diverse group of diseases that can originate in almost any tissue or organ in the human body. According to the World Health Organization [33], it is a major global health issue, responsible for almost 10 million deaths in 2020. The most frequently diagnosed cancers in 2020 were breast (2.26 million cases), lung (2.21 million cases), colorectal (1.93 million cases), prostate (1.41 million cases), skin (non-melanoma, 1.20 million cases), and stomach (1.09 million cases). Meanwhile, the cancers causing the highest number of deaths were the lung

⋆ corresponding author

ICCS Camera Ready Version 2025
To cite this paper please use the final published version:
DOI: 10.1007/978-3-031-97554-7_31

(1.80 million deaths), colorectal (916,000 deaths), liver (830,000 deaths), stomach (769,000 deaths), and breast (685,000 deaths) [33]. Figure 1A shows that, in women, breast cancer is the leading cause in several countries. Furthermore, in Brazil, the breast cancer death rate in women is increasing in contrast with developed countries such as Germany, France, the USA, and Canada, as shown in Fig. 1B [4].

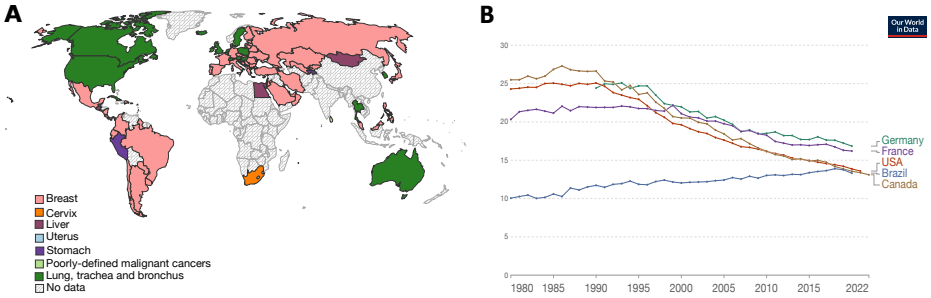

Fig. 1. A Leading cancer types causing death in women in 2022; and **B** Breast cancer death rate in women. Adapted from Our World in Data [4]

Effective cancer treatment requires accurate diagnosis and tailored therapies. Common approaches include surgery, radiotherapy, and systemic treatments such as chemotherapy and targeted therapies [19].

Hyperthermia, explored since the 1950s [6], is a promising non-invasive cancer treatment that eliminates tumor cells by raising tissue temperatures to induce necrosis [15]. It is often used to complement chemotherapy and radiotherapy, especially in treating liver [14] and breast tumors [11].

One strategy for hyperthermia involves using a magnetic nanoparticles ferrofluid. These nanoparticles generate heat when submitted to an alternating magnetic via Néelian and Brownian relaxation mechanisms [16, 17, 26].

Despite being explored for decades [6], hyperthermia remains in the early stages of development, leaving numerous questions open for investigation. Mathematical models and computational simulations provide valuable tools for studying and optimizing this treatment. Several models have been formulated to analyze heat transfer in biological tissues [13, 20, 25]. In this study, we employ a bioheat model proposed by Pennes [23]. Although this model was proposed in 1948, several studies use this bioheat approach because it offers a reasonable approximation with a low computational cost [1, 5, 20]. Since models like the Pennes bioheat equation rely on partial differential equations (PDEs), numerical methods are required for their solution. Here, we employ a Forward Time Centered Space (FTCS) scheme to compute the numerical solution, considering a heterogeneous medium.

The Arrhenius model is fundamental in evaluating thermal damage in biological tissues during hyperthermia treatments for cancer [3, 30]. It describes

ICCS Camera Ready Version 2025
To cite this paper please use the final published version:
DOI: 10.1007/978-3-031-97554-7_31

the relationship between temperature and reaction rates, explaining biochemical and structural alterations caused by heat. Key parameters, such as the frequency factor (A) and activation energy (E_a), govern tissue sensitivity to temperature changes. The frequency factor reflects the likelihood of molecular interactions, while activation energy represents the threshold energy required for transformations. These experimentally determined parameters quantify cumulative thermal damage, expressed as thermal dose, which helps maximize tumor cell destruction while minimizing harm to healthy tissues. Integrating bioheat models with computational simulations of cellular responses enhances the precision and safety of hyperthermia protocols, optimizing treatment outcomes.

The stochastic nature of E_a and A reflects biochemical variability across tumor types, stages, and patient-specific factors [10]. To assess the reliability of thermal damage models, we employ uncertainty quantification (UQ), focusing on E_a and A in the Arrhenius equation. Specifically, we investigate how variations in these parameters — shaped by tissue composition, tumor heterogeneity, and experimental conditions [12, 34] — affect predictions of cumulative thermal damage. In this context, the Monte Carlo method is used for uncertainty analysis in hyperthermia cancer treatment within both simulation and experimental contexts [2, 29], and it is also employed for sensitivity analysis in the Arrhenius model [18]. So, we employ Monte Carlo (MC) simulations to quantify the uncertainty of the results, considering E_a and A as random variables defined by probability density functions (PDFs) using values found in the literature. Incorporating these uncertainties allows for a more robust prediction framework, which offers insights into the reliability and range of the results of hyperthermia treatment. So, to the best of our knowledge, no previous studies have analyzed how these uncertain inputs might affect the Arrhenius model approach for thermal damage and how it might compromise simulations of hyperthermia for cancer treatment.

Solving PDEs in three-dimensional domains with UQ introduces significant computational challenges. This work uses CUDA to speed up the computational time required to solve the PDE model. This strategy enables efficient computation, significantly reducing the time required to obtain solutions while maintaining scalability and reliability.

We organise this paper as follows. Section 2 describes the bioheat model, numerical approximation and the uncertainty quantification. The results are presented in section 3 and discussed in section 4. Finally, section 5 presents the conclusions and plans for future work.

2 Methods

2.1 Mathematical Model

The heat transfer within living tissues can be described using the Pennes bioheat equation, expressed as:

$$\rho c \frac{\partial T}{\partial t} = \nabla \cdot k \nabla T + \omega_b \rho_b c_b (T_a - T) + Q_m + Q_r, \tag{1}$$

ICCS Camera Ready Version 2025
To cite this paper please use the final published version:
DOI: 10.1007/978-3-031-97554-7_31

where T represents the tissue temperature, and T_a corresponds to the blood core temperature. The parameters ρ, c, and k denote the density, specific heat, and thermal conductivity, respectively. Similarly, ρ_b, c_b, and ω_b represent the blood's density, specific heat, and perfusion rate, respectively. Lastly, Q_m accounts for the generation of metabolic heat, while Q_r represents the heat produced by magnetic nanoparticles.

Heat generation from magnetic nanoparticles can be modeled using data from an *in vivo* experiment on rat hind limbs [28], which provides a method for estimating the specific absorption rate (SAR) near the injection site, based on the properties of a ferromagnetic fluid with 0.1, 0.2 or 0.3 cc injected. Heat generation is expressed as $Q_r(\boldsymbol{x}) = \sum_{i=1}^{N} A_i e^{-r_i^2/r_{0,i}^2}$, where N denotes the number of nanoparticle injections, A_i is the maximum heat generation rate for the i-th injection, r_i is the distance from the i-th injection point, and $r_{0,i}$ is the hyperthermia coverage radius for the i-th injection.

Finally, the well-posed problem, including appropriate boundary and initial conditions, is formulated as follows:

$$\begin{cases} \rho c \dfrac{\partial T}{\partial t} = \nabla \cdot k \nabla T + \omega_b \rho_b c_b (T_a - T) + Q_m + Q_r & \text{in } \Omega \times I, \\ k \nabla T \cdot \boldsymbol{n} = 0 & \text{in } \partial\Omega \times I, \\ T(\cdot, 0) = 37, 0 & \text{in } \Omega, \end{cases} \tag{2}$$

where $\Omega \subset \mathbb{R}^3$ represents the spatial domain, $I \subset \mathbb{R}^+$ denotes the time domain, and $T : \Omega \times I \to \mathbb{R}^+$ is the tissue temperature field.

2.2 Numerical Scheme

The finite difference method (FDM) is applied to solve Eq. (2), making it a suitable approach for addressing this bioheat transfer problem. The heterogeneous medium is defined within a closed domain Ω, which is discretized into a uniform grid of points $\{(x_i); i = 0, 1, \ldots, N_x\}$, where N_x represents the number of intervals in the spatial dimension x, with a spacing of h. This discretization process is extended to other spatial dimensions. Similarly, the time domain I is divided into N_t intervals of equal size h_t, resulting in a time grid denoted as $S_I = \{(t_n); n = 0, 1, \ldots, N_t\}$. The governing equation is then discretized using a Forward Time Centered Space (FTCS) scheme.

The explicit FDM formulation is expressed as:

ICCS Camera Ready Version 2025
To cite this paper please use the final published version:
DOI: 10.1007/978-3-031-97554-7_31

$$T_{x,y,z}^{n+1} = \frac{h_t}{\rho c}\Bigg[\frac{k_{x+1/2,y,z}(T_{x+1,y,z}^n - T_{x,y,z}^n) - k_{x-1/2,y,z}(T_{x,y,z}^n - T_{x-1,y,z}^n)}{h^2} + \frac{k_{x,y+1/2,z}(T_{x,y+1,z}^n - T_{x,y,z}^n) - k_{x,y-1/2,z}(T_{x,y,z}^n - T_{x,y-1,z}^n)}{h^2} + \frac{k_{x,y,z+1/2}(T_{x,y,z+1}^n - T_{x,y,z}^n) - k_{x,y,z-1/2}(T_{x,y,z}^n - T_{x,y,z-1}^n)}{h^2} + \rho_b c_b \omega_b (T_a - T_{x,y,z}^n) + Q_m + Q_r\Bigg] + T_{x,y,z}^n, \tag{3}$$

where this scheme has linear convergence, $O(h_t)$, in time and quadratic convergence, $O(h^2)$, in space.

In the FDM framework, the thermal conductivity k varies across the domain Ω, making its evaluation at cell interfaces, such as $k_{i+1/2,j,k}$, crucial for accurate heat flux calculations, especially in heterogeneous media with abrupt changes in thermal properties. To address this, the harmonic mean is employed to compute the thermal conductivity at cell interfaces, ensuring flux continuity and capturing correct heat transfer behavior in piecewise homogeneous media. For the x-axis, this is expressed as $k_{i+1/2,j,k} \approx 2k_{i,j,k}k_{i+1,j,k}/(k_{i,j,k} + k_{i+1,j,k})$, with the same approach applied for all other midpoints in the computational domain. Additionally, the stability condition outlined in our previous work [25] is used to determine the time step h_t.

2.3 Thermal Damage

To assess the extent of thermal damage in both tumor and healthy regions, the Arrhenius model, expressed in Eq. 4, is applied. This model integrates the local temperature history to estimate tissue viability, considering the biochemical reactions triggered by heat exposure. The damage integral quantifies the fraction of cells affected, dependent on both exposure time and temperature intensity:

$$\Omega_A(x,y,z,t) = \ln\left(\frac{C(0)}{C(t)}\right) = \int_0^t A e^{\frac{-E_a}{R_u T(x,y,z,\tau)}}\, d\tau. \tag{4}$$

In this equation, A is the frequency factor, indicating the probability of molecular collisions that lead to irreversible damage. The activation energy E_a represents the minimum energy required to initiate the damage process. The universal gas constant R_u establishes a relationship between energy and temperature. The temperature $T(x,y,z,\tau)$ defines the absolute tissue temperature at a specific location over time, while τ corresponds to the duration of exposure. The concentrations $C(0)$ and $C(t)$ denote the initial and remaining viable cell populations, respectively, allowing an estimation of the progression of thermal damage.

ICCS Camera Ready Version 2025
To cite this paper please use the final published version:
DOI: 10.1007/978-3-031-97554-7_31

The computed damage parameter Ω_A provides a measure of cumulative tissue injury, where higher values indicate significant and irreversible cell loss. An Arrhenius damage parameter of 1.0 correlates with approximately 63.2% cell death, whereas a value of 4 suggests nearly 98.2% cell death [9]. Studies indicate that values exceeding 10 lack physical significance [22], and a range of $4 \leq \Omega_A \leq 10$ is commonly accepted as a criterion for complete tumor ablation [24].

2.4 Uncertainty Quantification

Uncertainty Quantification (UQ) [31] is a critical tool for assessing the sensitivity and reliability of computational models. By incorporating uncertainties in input parameters, UQ evaluates their impact on model outputs, thereby enhancing the credibility of predictions and supporting informed decision-making in complex systems. This approach systematically elucidates how input variability influences simulation results, ultimately improving model reliability.

Among UQ techniques, the Monte Carlo (MC) method is widely employed to address complex problems involving parameter interactions [31]. By using random sampling based on probability density functions (PDFs), MC simulations systematically explore the system's response under varying inputs. This method captures a broad range of scenarios and provides insights into central tendencies, variability, and the likelihood of specific outcomes. In this work, the MC method is applied to quantify uncertainties arising from inaccuracies in injection positioning during hyperthermia-based treatments for non-specific cancers.

Additionally, the MC method is used to quantify uncertainties associated with the two empirical parameters in the Arrhenius model. Experimental observations reveal a mutual correlation between the frequency factor A and the activation energy E_a, as expressed by Eq. (5) and Eq. (6) [7,8]:

$$E_a \approx 2.63 \times 10^3 ln(A) + 2.46 \times 10^4, \tag{5}$$

$$ln(A) = 3.832 \times 10^{-4} E_a - 10.042. \tag{6}$$

Extensive research has documented a wide range for these parameters, with the frequency factor A spanning from $A_{min} = 7.39 \times 10^{39}$ to $A_{max} = 3.10 \times 10^{98}$, and the activation energy E_a ranging from $E_{a_{min}} = 2.577 \times 10^5$ J/mol to $E_{a_{max}} = 6.030 \times 10^5$ J/mol [21,32]. These variations underscore the complexity of accurately modeling thermal damage in biological tissues and highlight the importance of selecting parameter values that reflect experimental conditions and tissue properties.

To evaluate the impact of the empirically observed variability in E_a and A, we perform hyperthermia treatment simulations by sampling values within their respective ranges. The activation energy E_a is sampled from a defined PDF, ensuring a comprehensive exploration of its variability. The empirical correlation between E_a and A is then used to determine the corresponding values of A.

ICCS Camera Ready Version 2025
To cite this paper please use the final published version:
DOI: 10.1007/978-3-031-97554-7_31

This method systematically assesses the uncertainties in these critical parameters, thereby providing a more robust understanding of treatment reliability and safety. The parameters are obtained via Eq. 7:

$$\begin{cases} E_{a_u} & = W \sim U(E_{a_{min}}, E_{a_{max}}), \\ A & = e^{3.832\times10^{-4}E_a - 10.042}, \end{cases} \tag{7}$$

and alternatively, the process can be performed in reverse using Eq. 8:

$$\begin{cases} A_u & = W \sim U(A_{min}, A_{max}), \\ E_a & = 2.63 \times 10^3 \ln(A_u) + 2.46 \times 10^4. \end{cases} \tag{8}$$

Here, $W \sim U(E_{a_{min}}, E_{a_{max}})$ denotes a uniform distribution between $E_{a_{min}}$ and $E_{a_{max}}$, while $W \sim U(A_{min}, A_{max})$ represents a uniform distribution between A_{min} and A_{max}. These unbiased sampling strategies facilitate a thorough analysis of how parameter-driven variations affect treatment outcomes.

3 Numerical Results

3.1 Computational Environment

The numerical solver was implemented in CUDA and compiled using `nvcc` version 12.6 with the `-O3` optimization flag, as described in Section 2.2. Moreover, the Monte Carlo (MC) algorithm described in Section 2.4 was implemented in the `C` programming language.

All computational experiments were performed on a system equipped with a 3.67 GHz AMD® EPYC™ 7713 CPU running Linux kernel version 4.18.0-477.15.1.el8_8.x86_64. The CPU features 128 physical cores. For CUDA acceleration, an NVIDIA A100 GPU based on the Ampere architecture was utilized, which provides 8,192 CUDA cores and 80 GB of HBM2e memory.

3.2 Simulation Scenario

This study examines the impact of the frequency factor (A) and the activation energy (E_a) on the calculation of the damage parameter Ω_A, which quantifies tissue damage induced by the hyperthermia process. The results are presented as the 95% confidence interval and the mean temperature after 50 minutes of hyperthermia therapy. A total of $1,000$ Monte Carlo samples were used to quantify the uncertainty in each parameter. For nanoparticle injections, a ferrofluid volume of 0.3 cc was considered, with a gel concentration of 0.5% and an infusion flow rate of 3μL/min.

The parameters for solving the Pennes bioheat equation are provided in Tables 1 and 2, with values adopted from the literature. The computational domain is modeled as a semi-sphere with a radius of 0.07 m, divided into seven concentric tissue layers of varying thicknesses. The outermost layer represents the epidermis (0.0001m thick), followed by the papillary dermis (0.0007m) and the reticular

ICCS Camera Ready Version 2025
To cite this paper please use the final published version:
DOI: 10.1007/978-3-031-97554-7_31

dermis (0.0008m). Next is the fat layer (0.005m thick), followed by glandular tissue (0.0434m), and finally muscle, which has a thickness of 0.015m. The tumor is modeled as a sphere located at $T(0.065, 0.065, 0.050)$ with a radius of 0.005m (see Figure 2). The spatial domain is uniformly discretized with $N_x = N_y = 256$ grid points in the x and y directions and $N_z = 128$ grid points in the z direction, while the time discretization is set to $h_t = 0.1$.

Two scenarios were considered to assess the significance of A and E_a in the evaluation of Ω_A. In the first scenario, A was randomly selected from the range reported in the literature using uniform distribution , and E_a was then computed using the corresponding empirical equation (Eq. (8)). In the second scenario, E_a was sampled from a uniform distribution based on scientific literature, and A was subsequently determined using the same empirical relationship (Eq. (7)).

Table 1. Parameter values used to solve Eq. (2) for the tissues. All parameter values were adapted from the literature [3].

Tissue	Thickness	k	ρ	c	Q_m	w_b
	(mm)	$(W/m^\circ C)$	(Kg/m^3)	$(J/Kg^\circ C)$	(W/m^3)	(s^{-1})
Epidermis	0.1	0.235	1200.0	3589.0	0.0	0.0002
Papillary Dermis	0.7	0.445	1200.0	3300.0	368.1	0.0013
Reticular Dermis	0.8	0.445	1200.0	3300.0	368.1	0.0013
Fat	5.0	0.210	930.0	2770.0	400.0	0.0013
Gland	43.4	0.480	1050.0	3770.0	700.0	0.0013
Muscle	15.0	0.480	1100.0	3800.0	700.0	0.0013
Tumor	10.0	0.480	1050.0	3852.0	5000.0	0.0013

Table 2. Parameter values used to solve SAR equation. All parameter values were adapted from the literature [27].

Parameters	Values	Unit
A	774.47×10^3	W/m^3
r_0	5.09×10^{-3}	m

3.3 Experiments

The solution of Eq. (2) is shown in Figure 3 and represents the temperature distribution at the end of the experiment (i.e., at $t = 50$min).

The analysis of thermal damage via the Arrhenius model is presented in Figures 4 and 5. Figures 4 show the scenario in which the uncertainty is characterized by A (using Eq. (8)), while Figures 5 correspond to the scenario where E_a is

ICCS Camera Ready Version 2025
To cite this paper please use the final published version:
DOI: 10.1007/978-3-031-97554-7_31

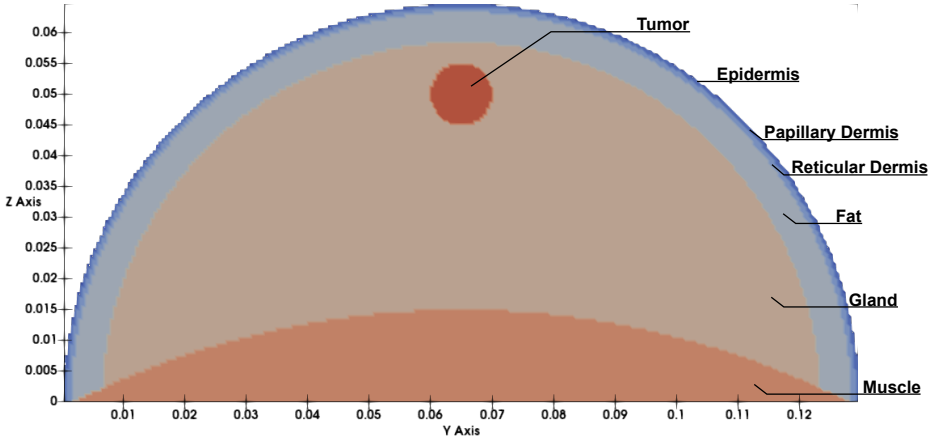

Fig. 2. Schematic representation of the computational domain for the hyperthermia simulation. The domain is modeled as a semi-sphere with a 0.07m radius, subdivided into seven concentric tissue layers representing the epidermis (0.0001m), papillary dermis (0.0007m), reticular dermis (0.0008m), fat (0.005m), glandular tissue (0.0434m), and muscle (0.015m). A spherical tumor (radius 0.005m) is positioned at $T(0.065, 0.065, 0.050)$. The spatial grid is uniformly discretized with $N_x = N_y = 256$ and $N_z = 128$ points.

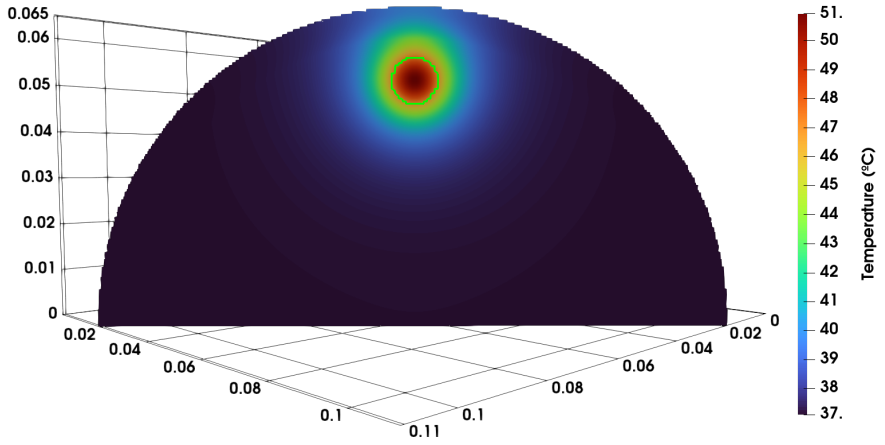

Fig. 3. Temperature distribution computed from the bioheat equation (Eq. (2)) at $t = 50$min. The solid green line delineates the tumor boundary.

treated as the uncertain parameter (using Eq. (7)). For both scenarios, the mean and 95% confidence intervals of Ω_A were evaluated at 5 minutes (Figures 4A and 5A), 10 minutes (Figures 4B and 5B), and at the end of the treatment (50 minutes; Figures 4C and 5C). In each figure, the left panel displays a cross-sectional

ICCS Camera Ready Version 2025
To cite this paper please use the final published version:
DOI: 10.1007/978-3-031-97554-7_31

view along the xy-plane with Ω_A values scaled between 0 and 10, while the right panel provides a zoomed-in view of the tumor area.

In the scenario where A is the uncertain parameter, after 5 minutes of hyperthermia treatment, the region where $\Omega_A \geq 4$ is confined to the center of the tumor (see Figure 4A). As the treatment progresses beyond 10 minutes (see Figure 4B), this threshold region expands, approaching the tumor boundary. Finally, after 50 minutes (see Figure 4C), the tumor exhibits Ω_A values exceeding 10, indicating significant tissue damage.

In the second scenario, the progression of Ω_A toward the target value is slower. As shown in Figure 5A, after 5 minutes of simulation, only the upper bound of the 95% confidence interval exhibits Ω_A values exceeding 4, while both the mean and the lower bound remain below this threshold, indicating minimal damage. In Figure 5B, the mean Ω_A value across 1,000 MC experiments reaches the target value, with the upper bound extending nearly to the tumor edge; however, the lower bound still falls below the threshold. Finally, Figure 5C demonstrates that at the end of the hyperthermia treatment (50 minutes), Ω_A reaches 10 or higher throughout the tumor region, signifying substantial tissue damage.

To further assess the impact of inaccuracies caused by variations in A and E_a, the mean temperature in both healthy and tumor tissues was evaluated every 5 minutes during the simulated treatment, as illustrated in Figures 6A and 6B. The results indicated that the minimum mean Ω_A in the tumor tissue exceeds 4, confirming that the entire tumor experiences significant damage, while the healthy tissue remains largely unaffected. Notably, Figure 6A shows that variations in A yield only minor differences, with a slight deviation observed at the 10-minute mark. In contrast, Figure 6B revels more pronounced variability during the first 30 minutes, with the damage region eventually converging such that 100% of the tumor tissue reaches the target Ω_A threshold.

4 Discussion

This work aimed to analyze how the Arrhenius model for thermal damage quantification responds to different parameter values reported in the literature. In our simulations, the damage parameter Ω_A reached the critical threshold ($\Omega_A \geq 4$) in the tumor region, indicating effective tissue damage, while healthy tissue experienced minimal side effects.

The numerical results revealed several important observations. First, even though the frequency factor A spans a vast range — from 10^{39} to 10^{98} — the outputs in Figure 4 show that both the mean values and the confidence intervals remain very close, even upon close inspection. This is further reinforced by Figure 6, which indicates almost no uncertainty in the outputs over time when A is treated as the uncertain parameter.

In contrast, variability in the activation energy E_a significantly impacts the Arrhenius model outputs. As shown in Figure 5, after 5 minutes the lower bound (2.5th percentile) and the mean Ω_A values are not visible because Ω_A remains

ICCS Camera Ready Version 2025
To cite this paper please use the final published version:
DOI: 10.1007/978-3-031-97554-7_31

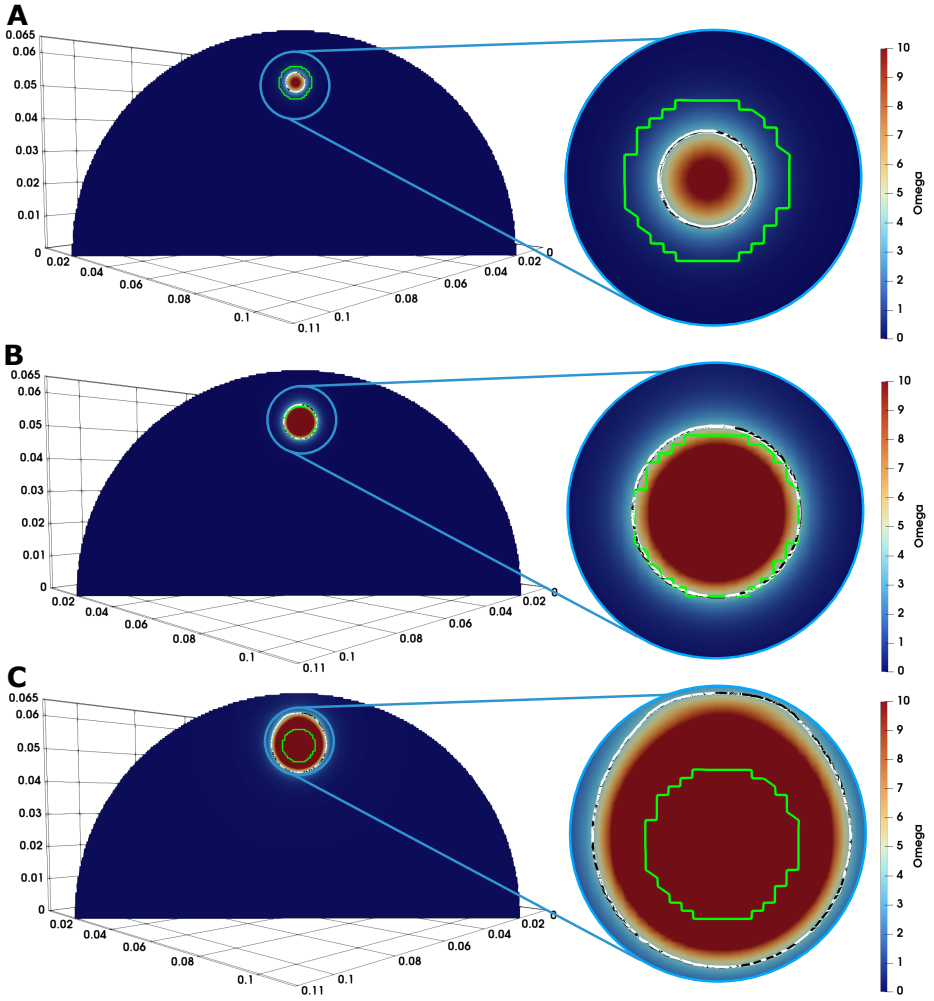

Fig. 4. Simulation results for the scenario with uncertainty in the frequency factor A. In all panels, the solid green line marks the tumor boundary, the solid white line delineates the upper and lower limits of the 95% confidence interval for Ω_A values at the threshold of 4, and the solid black line indicates the mean Ω_A values exceeding 4. Panels A, B, and C show the Ω_A distribution in the computational mesh after 5, 10, and 50 minutes of hyperthermia treatment, respectively.

below 4 across the domain. However, as the treatment progresses, Ω_A begins to increase, and the mean value becomes apparent in Figure 6 as Ω_A exceeds 4. Ultimately, Figure 6 demonstrates that all metrics reach $\Omega_A \geq 10$ in the tumor area. Although there is considerable variability, the results consistently indicate that sufficient damage is inflicted on the cancerous tissue.

ICCS Camera Ready Version 2025
To cite this paper please use the final published version:
DOI: 10.1007/978-3-031-97554-7_31

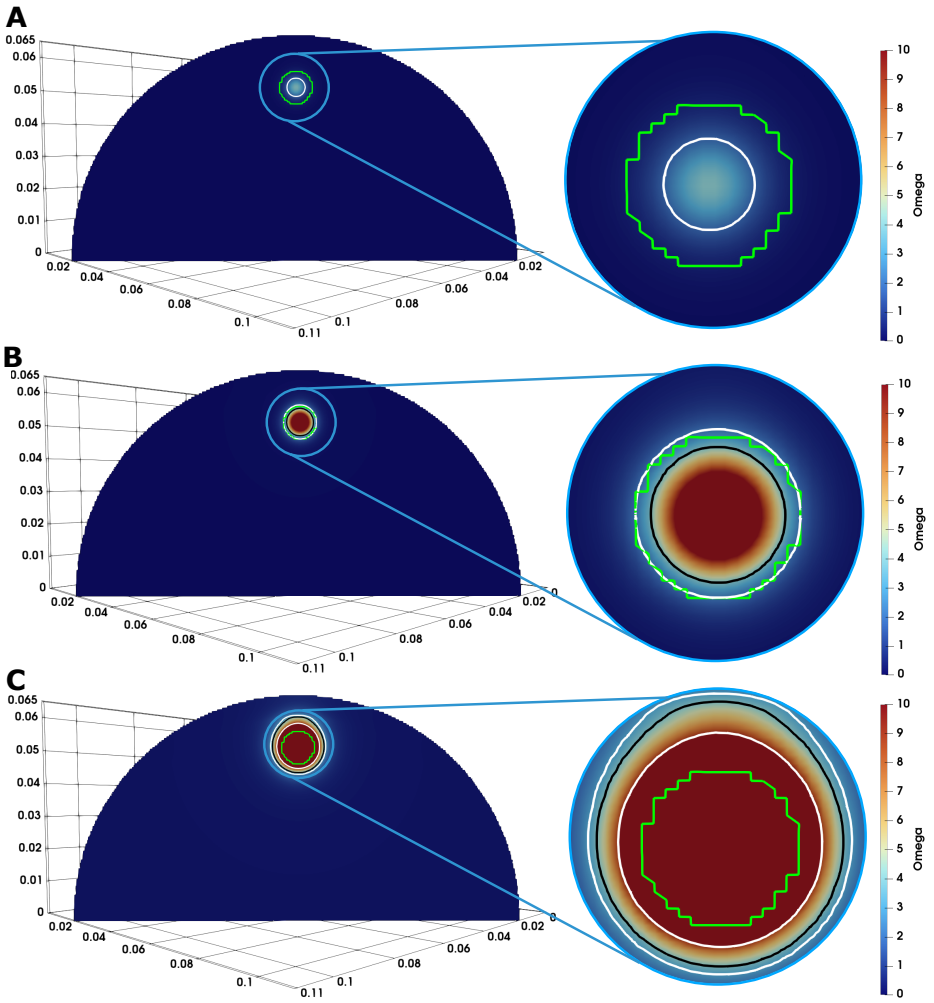

Fig. 5. Simulation scenario considering the uncertainty in the activation energy (E_a). In all panels, the solid green line represents the tumor boundary, the solid white line delineates the upper and lower bounds of the 95% confidence interval for Ω_A values reaching 4, and the solid black line indicates the mean Ω_A values exceeding 4.

5 Conclusions and Future Works

This work demonstrates the impact of variations in the frequency factor (A) and the activation energy (E_a) on the Arrhenius model used to evaluate thermal damage. A three-dimensional breast tissue model was employed to perform uncertainty quantification via Monte Carlo simulations for hyperthermia cancer treatment, treating A and E_a as random variables characterized by probability density functions.

ICCS Camera Ready Version 2025
To cite this paper please use the final published version:
DOI: 10.1007/978-3-031-97554-7_31

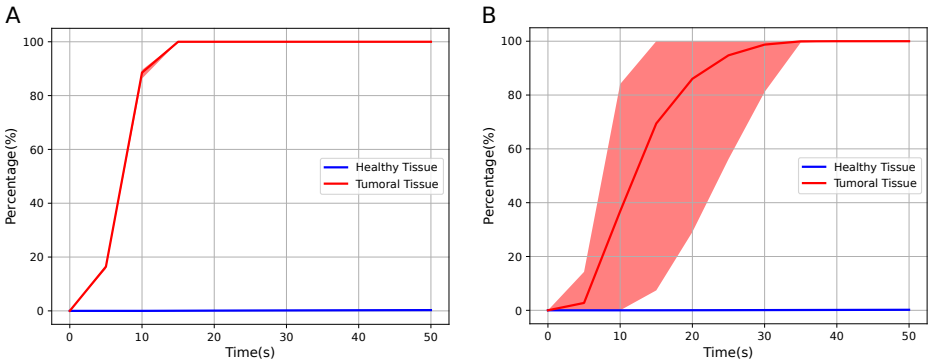

Fig. 6. Results of the uncertainty quantification caused by variations in A and E_a for assessing tumor damage during hyperthermia. The solid line represents the mean percentage of the tumor region where $\Omega_A \geq 4$, while the shaded area indicates the 95% confidence interval based on $1,000$ MC samples. Panel A corresponds to the first scenario, where E_a is derived from the uncertainty in A. In contrast, Panel B represents the opposite scenario, where A was calculated from variations in E_a.

Numerical results reveal that variations in the activation energy A have a minor influence on tissue damage predictions, whereas variations in the activation energy E_a significantly affect the outcomes. In particular, the wide confidence intervals observed in the thermal damage outputs indicate that uncertainty in E_a can result in a rapid rise (approximately 15 minutes) or a slower increase (up to 35 minutes) to reach the critical damage threshold ($\Omega_A \geq 4$).

In future work, we plan to incorporate Multigrid Monte Carlo (MGMC) methods to accelerate simulations and improve computational efficiency. Traditional Monte Carlo methods often suffer from slow convergence and high computational costs, particularly in high-dimensional problems. In our study, analyzing the influence of A and E_a required approximately 18 hours per simulation. MGMC addresses these challenges by leveraging a hierarchy of grid levels to enhance sampling efficiency. Integrating MGMC is expected to reduce computational time while maintaining accuracy, thereby enabling more complex and large-scale simulations. Furthermore, we intend to validate the model results with clinical or experimental data.

Acknowledgments. The authors would like to express their thanks to CAPES (Finance Code 001 and Projeto CAPES - Processo 88881.708850/2022-01), CNPq (308745/2021-3), FAPEMIG (APQ-02830/17 and APQ-01226-21), FINEP (SOS Equipamentos 2021 AV02 0062/22) and UFJF for funding this work.

Disclosure of Interests. The authors have no competing interests to declare that are relevant to the content of this article.

ICCS Camera Ready Version 2025
To cite this paper please use the final published version:
DOI: 10.1007/978-3-031-97554-7_31

References

1. Alpers, J., Rötzer, M., Gutberlet, M., Wacker, F., Hensen, B., Hansen, C.: Adaptive simulation of 3d thermometry maps for interventional mr-guided tumor ablation using pennes' bioheat equation and isotherms. Scientific Reports **12**(1) (Nov 2022)
2. Aono, C.M., Aquino, V.R.R., Bakuzis, A.F., Miotto, R.: Kinetic monte carlo approach as a tool for the study of magnetic hyperthermia efficiency. The Journal of Physical Chemistry C **129**(1), 927–939 (Dec 2024)
3. Cao, T.L., Le, T.A., Hadadian, Y., Yoon, J.: Theoretical analysis for using pulsed heating power in magnetic hyperthermia therapy of breast cancer. Int. J. Mol. Sci. **22**(16), 8895 (2021)
4. Dattani, S., Samborska, V., Ritchie, H., Roser, M.: Cancer. Our World in Data (2024), https://ourworldindata.org/cancer
5. Fatigate, G.R., Lobosco, M., Reis, R.F.: A 3D approach using a control algorithm to minimize the effects on the healthy tissue in the hyperthermia for cancer treatment. Entropy **25**(4), 684 (Apr 2023). https://doi.org/10.3390/e25040684
6. Gilchrist, R.K., Medal, R., Shorey, W.D., Hanselman, R.C., Parrott, J.C., Taylor, C.B.: Selective inductive heating of lymph nodes. Annals of Surgery **146**(4), 596–606 (1957)
7. He, X.: Thermostability of biological systems: fundamentals, challenges, and quantification. Open Biomed. Eng. J. **5**(1), 47–73 (Apr 2011)
8. He, X., Bischof, J.C.: Quantification of temperature and injury response in thermal therapy and cryosurgery. Crit. Rev. Biomed. Eng. **31**(5-6), 355–422 (2003)
9. Henriques, F.C., Moritz, A.R.: Studies of thermal injury: I. the conduction of heat to and through skin and the temperatures attained therein. a theoretical and an experimental investigation. The American journal of pathology **23**(4), 530–549 (1947)
10. Hicklin, D.J., Ellis, L.M.: Role of the vascular endothelial growth factor pathway in tumor growth and angiogenesis. Journal of clinical oncology **23**(5), 1011–1027 (2005)
11. Hilger, I., Hergt, R., Kaiser, W.A.: Towards breast cancer treatment by magnetic heating. Journal of Magnetism and Magnetic Materials **293**(1), 314 – 319 (2005), proceedings of the Fifth International Conference on Scientific and Clinical Aplli-cations of Magnetic Carriers
12. Ishida, H., Hachiga, T., Andoh, T., Akiguchi, S.: In-vivo visualization of melanoma tumor microvessels and blood flow velocity changes accompanying tumor growth. Journal of Applied Physics **112**(10), 104703 (2012)
13. Khaled, A.R., Vafai, K.: The role of porous media in modeling flow and heat transfer in biological tissues. International Journal of Heat and Mass Transfer **46**(26), 4989 – 5003 (2003)
14. Matsuki, H., Yanada, T., Sato, T., Murakami, K., Minakawa, S.: Temperature-sensitive amorphous magnetic flakes for intratissue hyperthermia. Materials Science and Engineering: A **181**(0), 1366 – 1368 (1994), proceedings of the Eighth International Conference on Rapidly Quenched and Metastable Materials: Part 2
15. Minkowycz, W., Sparrow, E.M., Abraham, J.P.: Nanoparticle heat transfer and fluid flow, vol. 4. CRC press (2012)
16. Moros, E.: Physics of thermal therapy: fundamentals and clinical applications. CRC Press (2012)
17. Moroz, P., Jones, S., Gray, B.: Magnetically mediated hyperthermia: current status and future directions. International Journal of Hyperthermia **18**(4), 267–284 (2002)

ICCS Camera Ready Version 2025
To cite this paper please use the final published version:
DOI: 10.1007/978-3-031-97554-7_31

18. Nagy, T., Turányi, T.: Uncertainty of arrhenius parameters. International Journal of Chemical Kinetics **43**(7), 359–378 (Apr 2011)
19. National Cancer Institute: Types of cancer treatment. `https://www.who.int/health-topics/cancer`. Last accessed 1 March 2025 (2025)
20. Ostadhossein, R., Hoseinzadeh, S.: The solution of pennes' bio-heat equation with a convection term and nonlinear specific heat capacity using adomian decomposition. Journal of Thermal Analysis and Calorimetry **147**(22), 12739–12747 (Jul 2022)
21. Paruch, M.: Identification of the degree of tumor destruction on the basis of the arrhenius integral using the evolutionary algorithm. Int. J. Therm. Sci. **130**, 507–517 (Aug 2018)
22. Pearce, J.A.: Comparative analysis of mathematical models of cell death and thermal damage processes. Int. J. Hyperthermia **29**(4), 262–280 (Jun 2013)
23. Pennes, H.H.: Analysis of tissue and arterial blood temperature in the restind human forearm. Journal of Applied Phisiology **1**, 93–122 (1948)
24. Prakash, P., Diederich, C.J.: Considerations for theoretical modelling of thermal ablation with catheter-based ultrasonic sources: implications for treatment planning, monitoring and control. Int. J. Hyperthermia **28**(1), 69–86 (2012)
25. Reis, R.F., dos Santos Loureiro, F., Lobosco, M.: 3D numerical simulations on gpus of hyperthermia with nanoparticles by a nonlinear bioheat model. Journal of Computational and Applied Mathematics **295**, 35–47 (2016)
26. Rosensweig, R.: Heating magnetic fluid with alternating magnetic field. Journal of Magnetism and Magnetic Materials **252**(0), 370 – 374 (2002), proceedings of the 9th International Conference on Magnetic Fluids
27. Salloum, M., Ma, R., Weeks, D., Zhu, L.: Controlling nanoparticle delivery in magnetic nanoparticle hyperthermia for cancer treatment: Experimental study in agarose gel. International Journal of Hyperthermia **24**(4), 337–345 (Jan 2008)
28. Salloum, M., Ma, R., Zhu, L.: An in-vivo experimental study of temperature elevations in animal tissue during magnetic nanoparticle hyperthermia. International Journal of Hyperthermia **24**(7), 589–601 (2008)
29. da Silva, N.P., Varon, L.A.B., da Costa, J.M.J., Orlande, H.R.B.: Monte carlo parameter estimation and direct simulation of in vitro hyperthermia-chemotherapy experiment. Numerical Heat Transfer, Part A: Applications **80**(5), 185–209 (Jul 2021)
30. Singh, M., Singh, T., Soni, S.: Pre-operative assessment of ablation margins for variable blood perfusion metrics in a magnetic resonance imaging based complex breast tumour anatomy: Simulation paradigms in thermal therapies. Comput. Methods Programs Biomed. **198**(105781), 105781 (jan 2021)
31. Smith, R.C.: Uncertainty Quantification: Theory, Implementation, and Applications. Society for Industrial and Applied Mathematics, Philadelphia, PA (2013). `https://doi.org/10.1137/1.9781611973228`
32. Soni, S., Tyagi, H., Taylor, R.A., Kumar, A.: The influence of tumour blood perfusion variability on thermal damage during nanoparticle-assisted thermal therapy. Int. J. Hyperthermia **31**(6), 615–625 (May 2015)
33. WHO: World health organization. `https://www.who.int/news-room/fact-sheets/detail/cancer`. Last accessed 23 March 2025 (2025)
34. Zhou, W., Chen, Z., Zhou, Q., Xing, D.: Optical biopsy of melanoma and basal cell carcinoma progression by noncontact photoacoustic and optical coherence tomography: In vivo multi-parametric characterizing tumor microenvironment. IEEE transactions on medical imaging **39**(6), 1967–1974 (2019)

ICCS Camera Ready Version 2025
To cite this paper please use the final published version:
DOI: 10.1007/978-3-031-97554-7_31